International Journal of Biological Macromolecules 154 (2020) 888–895

Contents lists available at ScienceDirect

International Journal of Biological Macromolecules

journal homepage: http://www.elsevier.com/locate/ijbiomac

Preparation and evaluation of alginate nanoparticles prepared by green method for drug delivery applications

Deepa Thomas [a,c], K. KurienThomas [a], M.S. Latha [b,c,*]

[a] Research and Post Graduate Department of Chemistry, Bishop Moore College, Mavelikara, Kerala, India
[b] Department of Chemistry, Sree Narayana College, Chengannur, Kerala, India
[c] Department of Chemistry, Sree Narayana College, Kollam, Kerala, India

ARTICLE INFO

Article history:
Received 18 June 2018
Received in revised form 10 February 2020
Accepted 19 March 2020
Available online 21 March 2020

Keywords:
Rifampicin
Honey
Alginate
Drug delivery
Biocompatibility

ABSTRACT

Nanosized natural polymers have attained considerable attention in drug delivery applications due to their high encapsulation efficiency, non-toxic nature, sustained and targeted drug delivery. Here we have synthesized Rifampicin loaded alginate nanoparticles by green method. Physicochemical characterization of the nanoparticles was assessed using Transmission electron microscopy, Fourier transform infrared spectroscopy, Dynamic light scattering and X-ray diffraction technique. The swelling and in vitro drug release showed that the framework experiences pH-dependent swelling and release of Rifampicin. Rifampicin has lower release in acid medium and higher release in intestinal condition. Moreover, in view of the drug release results, the release kinetics and transport mechanisms were investigated and discussed. In vitro cytotoxicity assay demonstrated that the nanoparticles were non-toxic in nature. The acute oral toxicity study of the synthesized nanoparticles was done in Wistar albino rats. No systemic toxicity was observed after oral administration of nanoparticles. The present study demonstrated the potential of using alginate nanoparticles synthesized by a green method for drug delivery applications.

1. Introduction

Nowadays the benefits and potential advantages which can be obtained from drug delivery systems using natural and synthetic polymers has gained a wide interest [1–6]. Natural polymers are considered as preferable drug carriers over synthetic materials because they possess several unique advantages such as hydrophilicity, biocompatibility and nontoxicity [7,8]. Among the different natural polymers, alginate (ALG) stands as one of the most advantageous biopolymers due to its low cost and easy availability [9]. The majority of the alginate particles portrayed in literature have micrometer dimension [10–13].

Nano sized drug delivery systems have numerous advantages such as targeted delivery, enhanced bioavailability, sustained drug release, improved patient compliance and reduced side effects [14]. The surface characteristics and particle size of nanoparticles can be easily tailored by varying the composition of polymers, drugs and other additives used in the formulation [15–17]. Particle size also assumes a pivotal part in intestinal uptake and in vivo distribution [18–20]. Panyam and his coworkers demonstrated that the particles below 100 nm were appeared to offer 15 to 250 fold cellular uptake than the micro particles using rat model study [21].The considerably high surface area of nanoparticles also guarantees significant payload [22–24].

Although, many methods for the preparation of alginate nanoparticles has been reported in the literature, including polyelectrolyte complexation, emulsification/internal gelation, solvent evaporation/diffusion and solvent-casting methods; however they have some limitations, such as porosity, difficult to reproduce, precipitation during the evaporation and use of volatile organic solvents [25]. Green chemistry principles could be adequately connected to the generation of ALG nanoparticles in a more secure and greener manner by avoiding organic solvents [26].Our group had developed a green method for the synthesis of highly stable, non-aggregate ALG nanoparticles of size above 100 nm using honey and demonstrated the potential of utilizing it for water purification [27–29]. In the present work, attempts were made to modify these nanoparticles suitable for drug delivery applications. Since particle size has a crucial role for drug delivery application, the preparation method was modified with the application of probe sonication. It was found that the high energy of probe sonication during the preparation stage of nanoparticles produced particles of smaller size [30].

Honey, an ancient pharmaceutical ingredient, rich in carbohydrate, has fantastic antioxidant, antibacterial, antifungal and anti-inflammatory properties. Ayurvedic medicine of India use honey

* Corresponding author at: Department of Chemistry, Sree Narayana College, Chengannur, Kerala, India.
E-mail address: lathams2014@gmail.com (M.S. Latha).

https://doi.org/10.1016/j.ijbiomac.2020.03.167
0141-8130/

predominantly as a vehicle for faster absorption of various drugs such as herbal extracts. It also supports the treatment of several ailments, particularly those related to respiratory irritations and infections, mouth sores and cataracts [4,31,32].The antibacterial and wound healing ability of honey gained much interest in the field of wound dressing [4,31,33]. This study was aimed to evaluate the potential of the alginate nanoparticles prepared by a green method using honey as the surfactant for drug delivery applications. Rifampicin (RIF), a high molecular weight bactericidal drug was used as the model drug.

RIF inhibits the growth of a broad spectrum of gram positive and gram negative bacteria, and is commonly used in the treatment of tuberculosis. It is the only drug which possesses the unique capacity to kill tubercular bacilli [34].The major challenges associated with RIF delivery are poor water solubility, short biological half-life and limited bioavailability. Anti-tuberculosis therapy is usually prolonged for a period more than six months and the conventional continuous uptake of drug causes adverse side effects including drug resistance, fever, hepatotoxicity and above all patient discomfort. In order to improve anti tuberculosis therapy, drug encapsulation in polymer nanoparticles has been widely studied. The subcutaneous route of administration experienced some drawbacks such as poor patient compliances [35,36] compared to the simple oral route of administration [37,38]. While considering the drawbacks of the other routes, oral administration of drugs is considered as the best alternative for long treatments of tuberculosis [36,39].

The objective of the present work was to develop biocompatible ALG nanoparticles of size <100 nm by green method for the oral delivery of RIF.

2. Experimental

2.1. Materials

Sodium alginate of medium viscosity (viscosity of 2% solution, 25 °C ≈ 3500 cps, Sigma-Aldrich, London), Rifampicin (Himedia Laboratories, Nasik), Calcium chloride dihydrate (Merck, Germany). Natural honey used in this study was purchased from Kerala Agriculture University.

2.2. Preparation of ALG nanoparticles

ALG nanoparticles were prepared by ionotropic gelation method as portrayed in our previous paper with slight modification [27]. Sodium alginate was dissolved in deionised water (1%, *w*/*v*) containing honey (added as a surfactant and stabilizer). RIF was dispersed in to this solution with continuous stirring. Aqueous calcium chloride (1%, *v*/v) solution was added drop wise to this solution, stirred and this homogenized mixture was sonicated. Nanoparticles ware harvested by centrifugation at 3500 rpm for 5 min, washed with deionised water and vacuum dried.

2.3. Characterizations of nanoparticles

The morphology of the ALG nanoparticles was observed by using a JEOL model 1200EX transmission electron microscope operated at an accelerating voltage at 80 kV. Fourier transform infrared (FTIR) spectra of RIF, sodium alginate and RIF loaded nanoparticles ware recorded between 400 and 4000 cm^{-1} wavelength range using Schimadzu FTIR model 1801. X-ray diffraction (XRD) patterns of the samples were recorded by using Brucker D8 Advance diffractometer with monochromatic Cu-Kα_1 radiation ($\lambda = 1.5418$ Å). The particle size and zeta potential measurements were carried out using a Zetasizer Nano ZSP instrument (Malvern, UK).

2.4. Entrapment efficiency of nanoparticles

The concentration of free RIF was estimated by noting the absorbance at 475 nm, using a UV–VIS spectrophotometer (PerkinElmer Lambda Bio 40). RIF content was determined by using the calibration curve fabricated from a series of solutions with known drug concentration. The entrapment efficiency percentage (% EE) was calculated as follows:

$$\%EE = \left(\frac{W_a - W_b}{W_a}\right) \times 100 \quad (1)$$

where W_a was the total weight of the drug fed and W_b was the weight of non-encapsulated free drug.

2.5. Swelling studies

Swelling of nanoparticles was determined by equilibrating a known mass of the nanoparticles with solvent and allowing them to swell to their equilibrium [40]. Accurately weighed dried ALG nanoparticles (100 mg) (W_d) were suspended in 10 ml solutions of different pH (1.2and 7.4) for 6 h in different bottles. At predetermined time intervals these bottles were taken and the swollen nanoparticles were collected by centrifugation at 10,000 rpm for 10 min (SORALL®BiogugeStratos Ultracentrifuge) and weighed immediately after removing the excess liquid carefully from the surface using filter paper (W_s). The percentage of swelling was estimated using Eq. (2). Data were expressed as mean ± standard deviation (SD) based on 3 independent measurements.

$$S = \left(\frac{W_s - W_d}{W_d}\right) \times 100 \quad (2)$$

2.6. In vitro drug release and release kinetics

In vitro drug release studies were performed in simulated gastric fluid (SGF, pH 1.2) and simulated intestinal fluid (SIF, pH 7.4) prepared according to the United States Pharmacopoeia at 37 °C under shaking conditions [41]. About 30 mg of each RIF loaded NPs formulations were taken in a dialysis bag of MW cut off 12,000 Da and was allowed to contact with 100 ml of the release medium. Aliquots were drawn at specific time intervals and replaced with equal volume of buffer. RIF concentration was determined from the absorbance at 475 nm in a UV–VIS spectrophotometer using the standard curve of RIF (PerkinElmer Lambda Bio 40). All experiments are conducted in triplicate and average value is taken.

To find out the drug release mechanism, the drug release data were analyzed using Korsmeyer–Peppas equation Eq. (3)

$$\frac{Qt}{Q\infty} = kt^n \quad (3)$$

Q_t/Q_∞ is fraction of drug released (<0.6) at time t, K is the rate constant and n is the release exponent. In this model, the value of n identifies the release mechanism of the drug. The values of these parameters vary with the geometric form of the system, that is, thin film, cylindrical or spherical. For a spherical system ≤0.43 indicates Fickian release and $n = 0.85$ indicates a purely relaxation-controlled delivery which is referred to as Case II transport. Intermediate values $0.43 < n < 0.85$ indicate an anomalous behaviour (non-Fickian kinetics corresponding to coupled diffusion/polymer relaxation) [42–44].

2.7. Evaluation of cell viability of ALG nanoparticles

Cell viability of ALG nanoparticles was studied using L929 fibroblast by MTT assay. The cells were refined with DMEM containing 10% FBS and the refined cell lines are kept at 37 °C in a humidified 5% CO_2

incubator for 24 h. The medium was then supplanted with test solution and incubated at 37 °C in a humidified 5% CO_2 incubator for specified time. Soon after, 30 μl of MTT (5 mg/ml) was added to the wells and incubated at 37 °C in a humidified 5% CO_2 incubator for 4 h. After the incubation period, the supernatant was evacuated and 100 μl DMSO was added to solubilize the formazan crystals. The absorbance values were measured by using micro plate reader at a wavelength of 570 nm to determine the optical density (OD). OD of control was obtained from the cells by repeating the above experiment without any sample. Cell viability (%) was calculated using Eq. (4)

$$Cell\ Viability(\%) = \left(\frac{OD\ of\ sample}{OD\ of\ control}\right) \times 100 \quad (4)$$

2.8. Acute toxicity studies

The acute toxicity of synthesized nanoparticles was evaluated in six adult female Wistar albino rats (8 to 12 weeks old, nulliparous and non-pregnant) weighing 210–230 g. The study was conducted following the Organization of Economic Co-operation and Development (OECD) guidelines for testing of chemicals (No. 420, Section 4: Health Effects) on conduct of "Acute Oral Toxicity – Fixed dose procedure" (Adopted: 17th December 2001) [45,46]. The Institutional Animal Ethics Committee of Confederation for Ayurvedic REnaissance-KERALAM LIMITED (CARe KERALAM LTD), Thrissur, Kerala, India has approved the experimental protocols (CKL/TOX/IAEC/2017-4/99). Animals were housed under standard laboratory conditions: air-conditioned environment with adequate fresh air supply through the IVC system, room temperature 21.0 to 24.0 °C, relative humidity 57–65%, with 12 h light and 12 h dark cycle. The temperature and relative humidity were recorded daily. ALG NPs administered through oral route to the animals using the rat gavaging needle as a single dose at an equivolume of 1 ml/100 g body weight for all animals and the actual volume of administration was calculated based on the most recent body weight of the animals. Using the normal procedure, a starting dose of 300 mg/kg followed by dosing of one animal at a higher dose level, 2000 mg/kg, serves the sighting study. In the main study further 4 animals were dosed at 2000 mg/kg. All animals were observed individually at least once during the first 30 min after dosing, then periodically during the first 24 h (with special attention during the first 4 h)and thereafter, daily for a total period of 14 days. Observations were made, including changes in skin and fur, eyes and mucous membranes, tremors, convulsions, salivation, diarrhoea, lethargy, sleep and coma and also respiratory, somatomotor activity and behaviour pattern in the animals. The body weight of each rat was recorded prior to treatment on Day 1, then weekly and at the terminal sacrifice time. Individual body weights and body weight changes were calculated. On 14th day all animals were sacrificed under euthanasia condition (overdose of thiopental sodium injection intraperitoneal) and were subjected to necropsy and gross pathologic examination.

3. Results and discussion

3.1. Preparation and characterization of nanoparticles

ALG NPs were prepared by simple ionic gelation technique. The whole preparation process utilized water as solvent and in this way stay away from the general issues of organic solvents. Honey, the remarkable regular 'nutritious supply' which has great biocompatibility, utilized as the stabilizer was the additional preferred advantage of the preparation. Concentration of honey is very critical in the formation of stable nanoparticles. At low concentration below 1%, aggregates were formed and above 1%, honey remained as separate droplets. A series of experiments were conducted to optimize the crosslinker concentration for nanopreparation. Concentration of $CaCl_2$ was varied from 0.5 to 4%,

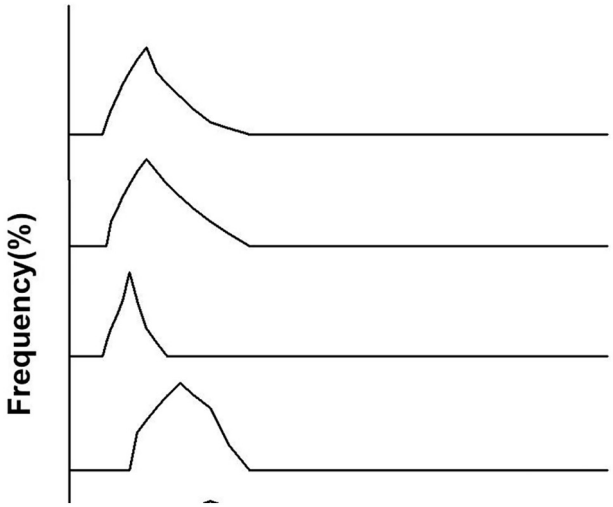

Fig. 1. Particle size distribution in different sonication time a) unsonicated b) 1 min c) 2 min d) 5 min e) 10 min f) 20 min.

keeping the concentrations of other components constant. Nanoparticles produced with >1% $CaCl_2$ concentration were not stable. $CaCl_2$ concentrations >1% resulted in the formation of nanoparticles of size above 100 nm. The well-defined spherical nanoparticles of suitable size for drug delivery application were formed at 1% $CaCl_2$ concentration. It was found that well defined spherical ALG nanoparticles were formed at a concentration of 1% (*w*/*v*) sodium alginate,1%(*v*/v) honey and 1% calcium chloride and selected for experiments. In order to evaluate the drug loading potential of the synthesized particle, the particle was loaded with RIF.

Mycobacterium tuberculosis was reported to start its replication inside the macrophages. Intracellular existence of mycobacterium and poor intracellular bioavailability of drug is the main cause of drug resistance in tuberculosis [47,48]. Encapsulation of drug in nanosized particles has tremendous potential in tuberculosis therapy as it enhances intracellular availability of drugs. Nanosized particles penetrate the cell wall and intracellular environment triggers the release of drug inside the cells. Small size and high surface volume ratio of the obtained ALG nanoparticles enhanced the solubility of RIF, allowing the targeted delivery and make it as an ideal carrier for RIF [49–51].

Effect of sonication on particle size was given in Fig. 1.The unsonicated sample exhibited a broad particle size distribution whereas an effective decrease in particle size with narrow size distribution was obtained as the sonication time increases up to 5 min. However, further increase in sonication time produced large particles. This behaviour can be related to the reaggregation of particles during prolonged sonication. These results are in accordance with previous reports [30,52]. Therefore five minute sonication was selected as optimum condition for nanoparticles preparation.

From Table 1, it was observed that drug loading does not alter much the particle size and zeta potential of ALG NP. The optimum drug-polymer ratio was found to be at 1:4.The entrapment efficiency of ALG nanoparticles could be explained on the basis of network structure produced during the cross linking of ALG with Ca^{2+} ions. In addition to this, RIF was dispersed into ALG solution and drug was loaded into the ALG

Table 1
Optimization parameters for RIF loaded ALG NP.

Formulation code	RIF: ALG	Drug entrapment efficiency % (% EE)	Particle size (nm)	Zeta potential (mV)
F1	1:2	36.58 ± 2.15	64 ± 22	−4.72 ± 0.17
F2	1:4	38.48 ± 2.85	65 ± 25	−4.85 ± 0.2
F3	1:6	35.94 ± 2.19	66 ± 20	−4.65 ± 0.19

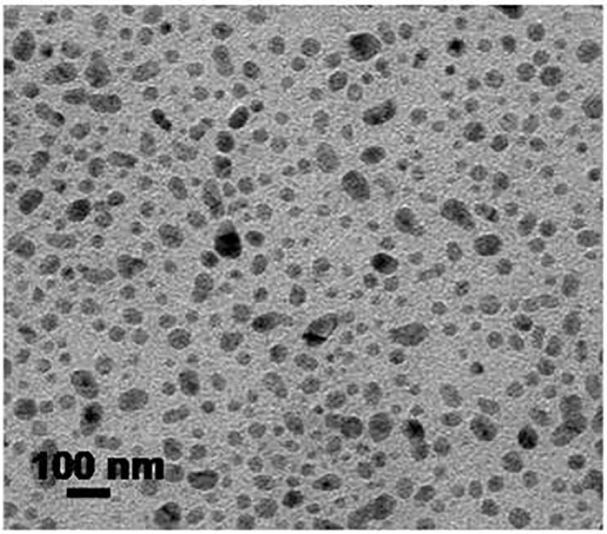

Fig. 2. TEM image of ALG NP.

matrix. The negative zeta potential indicates the presence of negative charge on the surface. The uncross-linked carboxylate group present in ALG is responsible for the negative charge. Since cell surface membranes are negatively charged, the positively charged nanoparticles created a destructive effect which tend to increase the cytotoxicity [53,54]. Our particles being slightly negative, it avoided such toxic interactions.

Shape and the morphology of the nanoparticles were investigated using TEM. From the TEM image (Fig. 2), it was observed that the nanoparticles exhibited a regular spherical shape with a mean size of 50–60 nm.

The FTIR spectrum of RIF, sodium alginate, ALG nanoparticles and RIF loaded ALG nanoparticles were given in Fig. 3. RIF shows characteristic bands at 3445 cm^{-1} (-OH), 1752 cm^{-1} (furanone), 1620 cm^{-1} (amide near C═O), 1580 cm^{-1} (C=C) and 1490 cm^{-1} (amide close to the C═C). In the spectrum of Na ALG, the peak at 3445 cm^{-1} assigned to the stretching vibration of hydroxyl groups (O—H). The peaks located at1026 cm^{-1} assigned to stretching vibration of C—O. Two characteristic absorption bands at 1628 cm^{-1} and 1418 cm^{-1}, which can be assigned to the asymmetric and symmetric stretching of COO–, respectively [55]. In ALG NPs, the bands corresponding to symmetric stretching of –COO showed a higher wave number shift with decrease in intensity. This higher wave number shift indicated the formation of ionic bonds between divalent calcium ion and -COO- of ALG. As Ca^{2+} ions replace sodium ions in the alginate blocks, the charge density, the radius and the atomic weight of the cations changed, thus creating a new environment around the carbonyl group. In the region 1150–1000 cm^{-1},a lower wave number shift was observed corresponding to the weakening of C—C and C—O bonds [56]. In RIF loaded ALG nanoparticles, the characteristic furanone peak at 1752 $cm^{-}1$ is overlapped with –COO- peak of ALG giving a band at 1662 cm^{-1}. These observations indicated that the incorporated drug has no chemical interaction with the polymer [57].

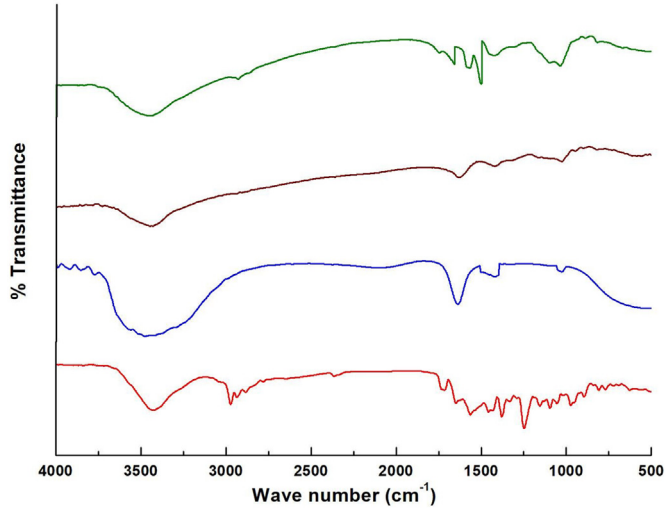

Fig. 3. FTIR of a) RIF b) Sodium ALG c) ALG nanoparticles d) RIF loaded ALG nanoparticles.

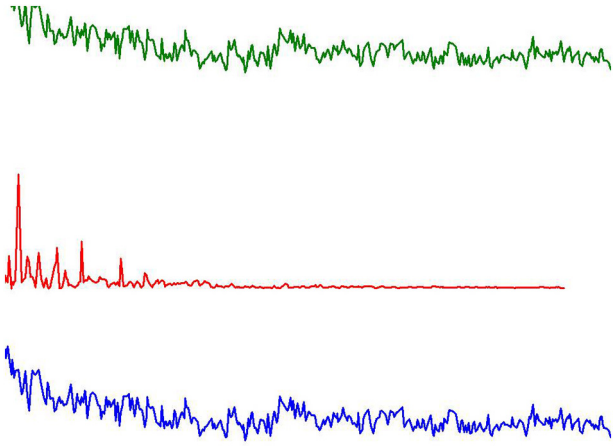

Fig. 4. XRD of a) ALG nanoparticles b) RIF c) RIF loaded ALG nanoparticles.

In RIF loaded ALG NPs, all the characteristic bands of drug were appeared. This indicated the chemical stability of RIF even after encapsulation into the polymer matrix and proved the absence of chemical interaction between RIF and polymer matrices.

XRD technique is utilized to analyze the nature of the drug in the carrier. XRD patterns of ALG nanoparticles, RIF and RIF loaded ALG nanoparticles were given in Fig. 4. The XRD pattern of RIF revealed its crystalline character from the major peaks at $2\theta = 13.65$ and 14.35 respectively [58]. Absence of sharp peaks in XRD of ALG nanoparticles confirmed their amorphous state. The characteristic peaks of RIF were not observed in RIF loaded ALG nanoparticles indicating that the drug is dispersed molecularly in the polymer matrix and almost complete amorphization of drug have occurred.

3.2. Swelling behaviour

The swelling behaviour of drug carrier affects the mechanism and kinetics of drug release. The swelling of Ca - ALG NPs was examined in simulated gastric fluid and intestinal fluid at room temperature as shown in Fig. 5. ALG is the assembly of β-d-mannuronic acid (M) and α -l-guluronic acid (G) units and can bind with divalent cations like Ca^{2+}, resulted in the formation of junction zones. This capacity makes ALG reasonable for enhancing mechanical properties, water vapour barrier and help to delay the release of drugs. From the figure it can be observed that the ALG nanoparticles exhibit a pH dependant swelling nature. This pH dependant swelling can be explained on the basis of its pKa value. ALG nanoparticles exhibit constrained swelling conduct at pH 1.2. It was found that if the pH value is less than the pKa of polymer, then most of the COOH groups get protonated, and form physical cross linking due to hydrogen bonding interaction between the neighbouring –COOH groups. The pKa value of ALG is 3.5. Hence in acidic medium (pH 1.2), the carboxylate groups of alginate were protonated and converted to insoluble alginic acid. There is a strong hydrogen bond interaction, which is responsible for the compact and impermeable polymer network structure. The percentage swelling of the nanoparticles was high in pH 7.4. At this pH which is above the pKa value, all the carboxylate groups of ALG are ionized and it increases

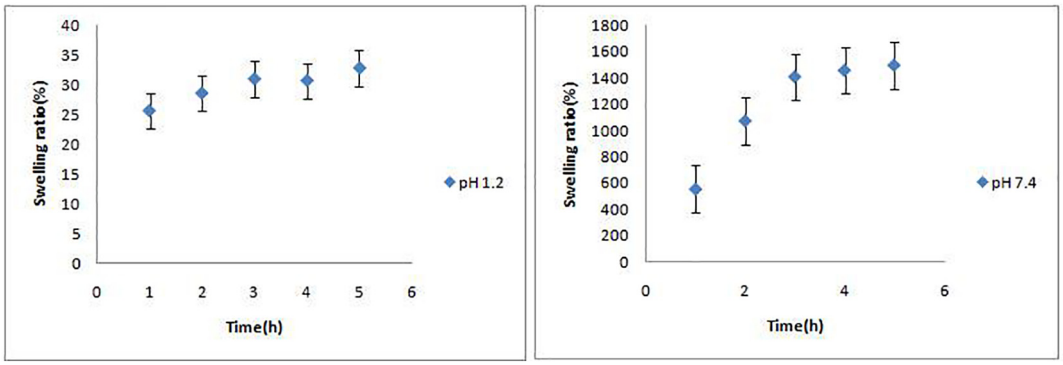

Fig. 5. Swelling behaviour of ALG NP (a) pH 1.2 (b) pH 7.4.

the electrostatic repulsion between ions. Moreover, an ion-exchange process occurs between the Ca^{2+} ions present in the "egg-box" cavity of poly guluronate blocks of ALG and Na^{+} ions of SIF, which enhances electrostatic repulsions among negatively charged carboxyl groups. Both the effects boost anionic density, increase the hydrophilicity of polymer and causes pronounced swelling, lead to chain relaxation and the gel swelling. These observations showed that ALG nanoparticles swell slightly in the stomach (pH 1.2) and swell significantly when it is transferred to the upper intestine (pH 7.4).

3.3. In vitro drug release and release kinetics

A pharmaceutical formulation intended to act in the intestine should be protected in the gastric environment. It must be absorbed through the gastrointestinal (GI) mucus layer and should maintain the therapeutic levels after reaching the targeting site. The degree of swelling determines the rate of drug release. In vitro drug release studies were performed in the fluids simulating the conditions of the GI tract for 2 h in SGF (pH 1.2) and 6 h in SIF (pH 7.4). From Fig. 6, it was found that the amount of drug released in SGF at pH 1.2 was very low. Only 10–25% of drugs was released within 2 h (the time expected to remain an orally administrated drug dosage form in the stomach). At this pH, these nanoparticles were not swollen much, the negative –COO group of calcium alginate protonated and acted as a diffusion barrier for the release of the drug. In vitro drug release was higher in the SIF compared to the SGF. At pH 7.4 a rapid increase in the release rate was observed up to 100% in 6 h. This increased release rate can be explained on the basis of the high degree of swelling, which is due to the deprotonation of alginic acid and ion exchange phenomenon. This pH dependant, sustained release of drug helps to maintain the concentration of RIF within therapeutic level and can avoid over dosage. The adhesive nature of ALG extends the contact time within the intestine and improves the absorption of drug and enhances its bioavailability. It was observed that all the three formulations possess almost same release pattern.

The drug-release kinetics for RIF from nano particle was analyzed fitting the release data with the Korsmeyer–Peppas (Table 2). By plotting ln Q_t/Q_∞ against ln t, get the value of the diffusion exponential (n). Analysis of release mechanism using Korsmeyer-Peppas equation analysis, prove that the system follows a Fickian transport mechanism for the first 2 h (pH 1.2). Here release is fully controlled by diffusion process. The value of n is found to be 0.54–0.57 for the time 2–4 h (pH 7.4). This indicated an anomalous behaviour of kinetics corresponding to coupled diffusion and swelling mechanism. The value of n changed to 0.41–0.42 for 4–6 h (pH 7.4). Here the drug release kinetics follow a purely diffusion mechanism. This behaviour can be explained on the basis of swelling characteristics of ALG NPs. On examining the swelling behaviour, it is observed that swelling reached a maximum after 3 h. Then drug was released from the fully swollen matrix by diffusion.

3.4. Evaluation of cell viability of ALG nanoparticles

For the fabrication and development of a drug delivery carrier, basic information about its biological safety is essential. In vitro

Table 2
Kinetic parameters of the drug release from ALG NP.

Time	K			n			R^2		
	F1	F2	F3	F1	F2	F3	F1	F2	F3
0–2 h	1.319	1.301	1.317	0.41	0.40	0.42	0.989	0.986	0.981
2–4 h	1.551	1.56	1.553	0.55	0.54	0.57	0.982	0.992	0.993
4–6 h	1.328	1.322	1.34	0.42	0.41	0.41	0.995	0.994	0.980

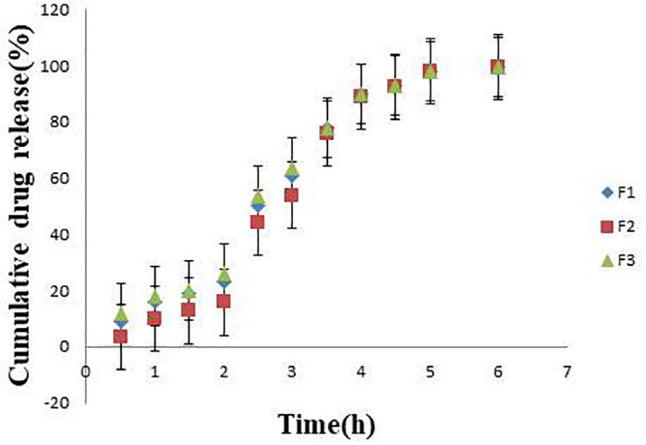

Fig. 6. Cumulative RIF release.

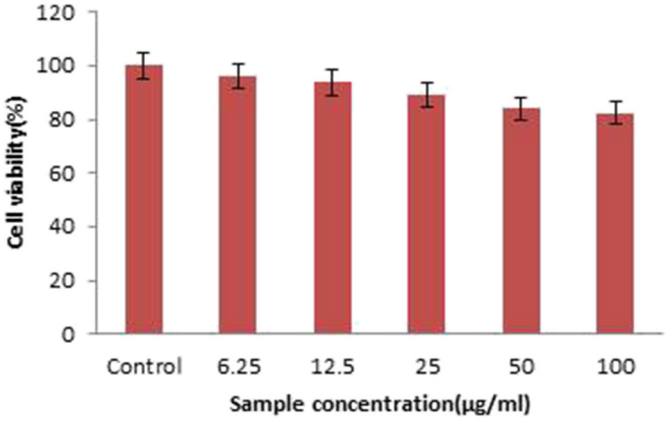

Fig. 7. The cell viability of L929 cells treated with ALG nanoparticles.

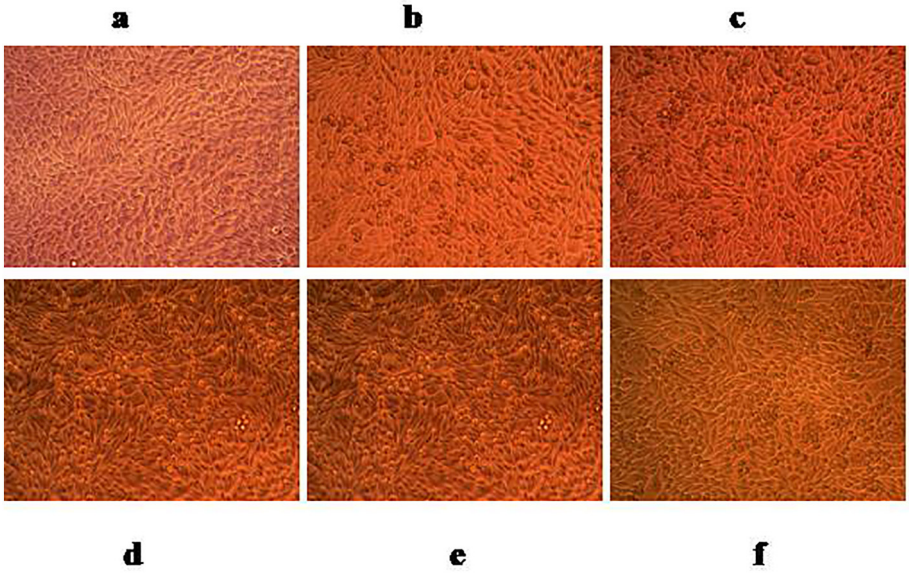

Fig. 8. Morphology of the L929 cells (a) Control cells (b) cells incubated with 6.25 μg/ml ALG NP (c) 12.5 μg/ml ALG NP (d) 25.0 μg/ml ALG NP (e) 50.0 μg/ml ALG NP (f) 100.0 μg/ml ALG NP (100×).

biocompatibility tests, such as cytotoxicity determination, are usually done to evaluate the biological safety of biomaterials [59]. In this study, cell culture method was selected for the preliminary evaluation of the biocompatibility of ALG NPs. The L929 mouse areolar/adipose fibroblasts was selected as target cell for this study since they were easy to cultivate and recommended as reference cell line for the cytotoxicity testing of polymers [59,60]. Cytotoxicity of ALG NP in L929 mouse fibroblasts was monitored using the 3-(4, 5-dimethylthiazol-2-yl)-2, 5-diphenyl tetrazolium bromide (MTT) assay. This test is based on the selective ability of viable cell to reduce MTT to non-water-soluble violet formazan crystals. The amount of formazan generated can be determined by spectrophotometrically and is directly proportional to the number of living, metabolically active cells. Thus the results of the MTT assay serve as an indicator of mitochondrial function and can use to evaluate the magnitude of cytotoxic effects of the sample. The results of the MTT assay, as an indicator of mitochondrial function. The cell viability was calculated as % of control cells. The viability of the cells was 100% for the control cells. Fig. 7 shows the percentage survival of L929 cells after exposure to the nanoparticles. L929 mouse fibroblasts are large, spindle-shaped, adherent cells growing as a confluent monolayer. Changes in cell morphology after treatment with nanoparticles were also used as indicators of cell survival by microscopic investigations. From Fig. 8, it was found that cells treated with 100.0 μg/ml of ALG NP, exhibited no significant differences from those of the control and no damage could be detected suggesting nanoparticles possess excellent biocompatibility.

3.5. Acute toxicity study of ALG NP

Investigation of the acute toxicity is the initial step in the toxicological examination of a substance. It involves qualitative and quantitative assessment of the toxic effects of a substance, and the evaluation of their time-related occurrence after single administration. The level of the acute toxicity is expressed as LD_{50}. It is the statistically derived amount of a substance that can be expected to cause death in 50% of the animals when given by a specified route as a single dose and the animals observed for a specified period of time. It provides useful pharmacologic and toxicological information [61,62]. The acute oral toxicity study of ALG NP in Wistar rats did not reveal any clinical signs, mortalities and gross pathological changes due to toxicity. The LD_{50} value of ALG NPs was found to be >2000 mg/kg. According to the globally harmonized system, chemical having LD_{50} value >2000 mg/kg, dose will come under "category 5" with toxicity rating "zero" [45]. Hence the developed ALG NP can be used as a promising carrier for oral drug delivery applications.

4. Conclusion

In the present study rapid, simple and green ionotropic gelation was proposed to prepare ALG nanoparticles. The probe sonication could effectively reduce the particle size suitable for drug delivery applications. In vitro drug release studies confirmed that the developed nanoparticles showed the property of pH-dependent release for RIF, and it was able to release most of RIF at pH value of 7.4. In vitro cytotoxicity assays revealed that this formulation is non-toxic. The acute toxicity studies revealed the absence of systemic toxicity and excellent safety after oral administration of nanoparticles. This study demonstrated that the developed nanoparticles make suitable as a good delivery system for controlled drug delivery applications.

Author statement

Deepa Thomas: Conceptualization, Methodology, Writing- Original draft preparation.
M.S. Latha: Supervision, Writing - Review & Editing.
Kurien Thomas: Supervision.

Declaration of competing interest

The Authors declare no conflict of interest.

Acknowledgements

This work was supported by the University Grants Commission (FIP/12th plan/KLKE002TF05).

The raw/processed data required to reproduce these findings cannot be shared at this time as the data also forms part of an ongoing study.

References

[1] A. Vashist, A. Vashist, Y.K. Gupta, S. Ahmad, Recent advances in hydrogel based drug delivery systems for the human body, J. Mater. Chem. B 2 (2014) 147–166, https://doi.org/10.1039/C3TB21016B.

[2] C. Pinto, F. Veiga, R.J. Neufeld, Nanoparticulate Delivery System for Insulin: Design, Characterization and in Vitro/in Vivo Bioactivity, 0, 2007 392–397, https://doi.org/10.1016/j.ejps.2006.12.007.

[3] S.C. Angadi, L.S. Manjeshwar, T.M. Aminabhavi, Interpenetrating polymer network blend microspheres of chitosan and hydroxyethyl cellulose for controlled release of isoniazid, Int. J. Biol. Macromol. 47 (2010) 171–179, https://doi.org/10.1016/j.ijbiomac.2010.05.003.

[4] X. Yang, L. Fan, L. Ma, Y. Wang, S. Lin, Green electrospun Manuka honey/silk fibroin fibrous matrices as potential wound dressing, Mater. Des. (2017) https://doi.org/10.1016/j.matdes.2017.01.023.

[5] L. Balaita, V. Maier, L. Verestiuc, M. Popa, Polymer nanoparticles for release of rifampicin, Adv. Sci. Eng. Med. 5 (2013) 96–104, https://doi.org/10.1166/asem.2013.1239.

[6] L. Peltonen, M. Karjalainen, J. Hirvonen, Effect of Nanoprecipitation on the Physicochemical Properties of Low Molecular Weight Poly (l-Lactic Acid) Nanoparticles Loaded With Salbutamol Sulphate and Beclomethasone Dipropionate, 295, 2005 269–281, https://doi.org/10.1016/j.ijpharm.2005.02.026.

[7] N.B. Shelke, R. James, C.T. Laurencin, S.G. Kumbar, Polysaccharide biomaterials for drug delivery and regenerative engineering, Polym. Adv. Technol. 25 (2014) 448–460, https://doi.org/10.1002/pat.3266.

[8] B. Lu, S. Bin Xiong, H. Yang, X.D. Yin, R.B. Zhao, Mitoxantrone-loaded BSA nanospheres and chitosan nanospheres for local injection against breast cancer and its lymph node metastases. I: formulation and in vitro characterization, Int. J. Pharm. 307 (2006) 168–174, https://doi.org/10.1016/j.ijpharm.2005.09.037.

[9] D. Jain, D. Bar-Shalom, Alginate drug delivery systems: application in context of pharmaceutical and biomedical research, Drug Dev. Ind. Pharm. 40 (2014) 1576–1584, https://doi.org/10.3109/03639045.2014.917657.

[10] J. Boekhoven, R.H. Zha, F. Tantakitti, E. Zhuang, R. Zandi, C.J. Newcomb, S.I. Stupp, Alginate–peptide amphiphile core–shell microparticles as a targeted drug delivery system, RSC Adv. 5 (2015) 8753–8756, https://doi.org/10.1039/C4RA16593D.

[11] R. Pandey, G.K. Khuller, Chemotherapeutic potential of alginate – chitosan microspheres as anti-tubercular drug carriers, J. Antimicrob. Chemother. 53 (2004) 635–640, https://doi.org/10.1093/jac/dkh139.

[12] S.K. Leslie, A.M. Nicolini, G. Sundaresan, J. Zweit, B.D. Boyan, Z. Schwartz, Development of a cell delivery system using alginate microbeads for tissue regeneration, J. Mater. Chem. B (2016) https://doi.org/10.1039/C6TB00035E.

[13] N. Patel, D. Lalwani, S. Gollmer, E. Injeti, Y. Sari, J. Nesamony, Development and evaluation of a calcium alginate based oral ceftriaxone sodium formulation, Prog. Biomater. 5 (2016) 117–133, https://doi.org/10.1007/s40204-016-0051-9.

[14] K.M. El-Say, H.S. El-Sawy, Polymeric nanoparticles: promising platform for drug delivery, Int. J. Pharm. 528 (2017) 675–691, https://doi.org/10.1016/j.ijpharm.2017.06.052.

[15] T.A. Debele, S.L. Mekuria, H.C. Tsai, Polysaccharide Based Nanogels in the Drug Delivery System: Application as the Carrier of Pharmaceutical Agents, Elsevier B.V., 2016https://doi.org/10.1016/j.msec.2016.05.121.

[16] A. Kakkar, G. Traverso, O.C. Farokhzad, R. Weissleder, R. Langer, Evolution of macromolecular complexity in drug delivery systems, Nat. Rev. Chem. 1 (2017) 1–18, https://doi.org/10.1038/s41570-017-0063.

[17] T. Garg, G. Rath, R.R. Murthy, U.D. Gupta, P.G. Vatsala, A.K. Goyal, Current nanotechnological approaches for an effective delivery of bioactive drug molecules to overcome drug resistance tuberculosis, Curr. Pharm. Des. 21 (2015) 3076–3089, https://doi.org/10.2174/1381612821666150531163254.

[18] D.E. Owens, N.A. Peppas, Opsonization, biodistribution, and pharmacokinetics of polymeric nanoparticles, Int. J. Pharm. 307 (2006) 93–102, https://doi.org/10.1016/j.ijpharm.2005.10.010.

[19] P.F. Minimol, W. Paul, C.P. Sharma, PEGylated starch acetate nanoparticles and its potential use for oral insulin delivery, Carbohydr. Polym. 95 (2013) 1–8, https://doi.org/10.1016/j.carbpol.2013.02.021.

[20] P. JANI, G.W. HALBERT, J. LANGRIDGE, A.T. FLORENCE, Nanoparticle uptake by the rat gastrointestinal mucosa: quantitation and particle size dependency, J. Pharm. Pharmacol. 42 (1990) 821–826, https://doi.org/10.1111/j.2042-7158.1990.tb07033.x.

[21] J. Panyam, V. Labhasetwar, Biodegradable nanoparticles for drug and gene delivery to cells and tissue, Adv. Drug Deliv. Rev. 55 (2003) 329–347, https://doi.org/10.1016/S0169-409X(02)00228-4.

[22] O. Kayser, A. Lemke, N. Hernandez-Trejo, The impact of nanobiotechnology on the development of new drug delivery systems, Curr. Pharm. Biotechnol. 6 (2005) 3–5, https://doi.org/10.2174/1389201053167158.

[23] M.P.A. Ferreira, V. Talman, G. Torrieri, D. Liu, G. Marques, K. Moslova, Z. Liu, J.F. Pinto, J. Hirvonen, H. Ruskoaho, H.A. Santos, Dual-drug delivery using dextran-functionalized nanoparticles targeting cardiac fibroblasts for cellular reprogramming, Adv. Funct. Mater. 28 (2018) 1–12, https://doi.org/10.1002/adfm.201705134.

[24] C. Zhang, Y. Guo, R.D. Priestley, Glass transition temperature of polymer nanoparticles under soft and hard confinement, Macromolecules. 44 (2011) 4001–4006, https://doi.org/10.1021/ma1026862.

[25] M. Lopes, B. Abrahim, F. Veiga, R. Seiça, M. Cabral, P. Arnaud, J.C. Andrade, A.J. Ribeiro, M. Lopes, B. Abrahim, F. Veiga, R. Seiça, M. Cabral, P. Arnaud, J.C. Andrade, A.J.R. Preparation, Preparation methods and applications behind alginate-based particles, Expert Opin. Drug Deliv.. 5247 (2016) https://doi.org/10.1080/17425247.2016.1214564.

[26] P.F. Andrade, A.F. De Faria, D. Soares, Structural and Morphological Investigations of β-Cyclodextrin-Coated Silver Nanoparticles, 20, 2014 2114–2115, https://doi.org/10.1017/S1431927614012306.

[27] P. Geetha, M.S. Latha, S.S. Pillai, B. Deepa, K. Santhosh Kumar, M. Koshy, Green synthesis and characterization of alginate nanoparticles and its role as a biosorbent for Cr(VI) ions, J. Mol. Struct. 1105 (2016) 54–60, https://doi.org/10.1016/j.molstruc.2015.10.022.

[28] P. Geetha, M.S. Latha, S.S. Pillai, M. Koshy, Nanoalginate based biosorbent for the removal of lead ions from aqueous solutions: equilibrium and kinetic studies, Ecotoxicol. Environ. Saf. 122 (2015) 17–23, https://doi.org/10.1016/j.ecoenv.2015.06.032.

[29] P. Geetha, M.S. Latha, M. Koshy, Biosorption of malachite green dye from aqueous solution by calcium alginate nanoparticles: equilibrium study, J. Mol. Liq. 212 (2016) 723–730, https://doi.org/10.1016/j.molliq.2015.10.035.

[30] P.D. Scholes, A.G.A. Coombes, L. Illum, S.S. Daviz, M. Vert, M.C. Davies, The preparation of sub-200 nm poly(lactide-co-glycolide) microspheres for site-specific drug delivery, J. Control. Release 25 (1993) 145–153, https://doi.org/10.1016/0168-3659(93)90103-C.

[31] W.A. Sarhan, H.M.E. Azzazy, I.M. El-sherbiny, The effect of increasing honey concentration on the properties of the honey/polyvinyl alcohol/chitosan nano fi bers, Mater. Sci. Eng. C 67 (2016) 276–284, https://doi.org/10.1016/j.msec.2016.05.006.

[32] P.M. Da Silva, C. Gauche, L.V. Gonzaga, A.C.O. Costa, R. Fett, Honey: chemical composition, stability and authenticity, Food Chem. 196 (2016) 309–323, https://doi.org/10.1016/j.foodchem.2015.09.051.

[33] W.A. Sarhan, H.M.E. Azzazy, High concentration honey chitosan electrospun nanofibers: biocompatibility and antibacterial effects, Carbohydr. Polym. 122 (2015) 135–143, https://doi.org/10.1016/j.carbpol.2014.12.051.

[34] W.L. Bragg, Development & evaluation of rifampicin formulation, Int. J. Adv. Pharmacy, Biol. Chem. (2011) 32–92.

[35] S. Azarmi, W.H. Roa, R. Löbenberg, Targeted delivery of nanoparticles for the treatment of lung diseases, Adv. Drug Deliv. Rev. 60 (2008) 863–875, https://doi.org/10.1016/j.addr.2007.11.006.

[36] J. Costa-Gouveia, J.A. Aínsa, P. Brodin, A. Lucía, How can nanoparticles contribute to antituberculosis therapy? Drug Discov. Today 22 (2017) 600–607, https://doi.org/10.1016/j.drudis.2017.01.011.

[37] D. Prabakaran, P. Singh, K.S. Jaganathan, S.P. Vyas, Osmotically regulated asymmetric capsular systems for simultaneous sustained delivery of anti-tubercular drugs, J. Control. Release 95 (2004) 239–248, https://doi.org/10.1016/j.jconrel.2003.11.013.

[38] A. Nokhodchi, S. Raja, P. Patel, K. Asare-Addo, The role of oral controlled release matrix tablets in drug delivery systems, BioImpacts. 2 (2012) 175–187, https://doi.org/10.5681/bi.2012.027.

[39] M. Kaur, T. Garg, R.K. Narang, A review of emerging trends in the treatment of tuberculosis, Artif. Cell Nanomed. Biotechnol. 44 (2016) 478–484, https://doi.org/10.3109/21691401.2014.962745.

[40] E. Al, G. Guclu, T.B. Iyim, S. Emik, S. Ozgumus, Synthesis and properties of starch-graft-acrylic acid/Na-montmorillonite superabsorbent nanocomposite hydrogels, J. Appl. Polym. Sci. 109 (2008) 16–22, https://doi.org/10.1002/app.

[41] U.S.P. Convention, US Pharmacopeia, XXV, 2002 2159.

[42] R.W. Korsmeyer, R. Gurny, E. Doelker, P. Buri, N.A. Peppas, Mechanisms of solute release from porous hydrophilic polymers, Int. J. Pharm. 15 (1983) 25–35, https://doi.org/10.1016/0378-5173(83)90064-9.

[43] P.L. Ritger, N.A. Peppas, A simple equation for description of solute release II. Fickian and anomalous release from swellable devices, J. Control. Release 5 (1987) 37–42, https://doi.org/10.1016/0168-3659(87)90035-6.

[44] P.L. Ritger, N.A. Peppas, A simple equation for description of solute release I. Fickian and non-fickian release from non-swellable devices in the form of slabs, spheres, cylinders or discs, J. Control. Release 5 (1987) 23–36, https://doi.org/10.1016/0168-3659(87)90034-4.

[45] OECD, Harmonized Integrated Classification System for Human Health and Environmental Hazards of Chemical Substances and Mixtures, No. 33, 2001 247 (doi:ENV/JM/MONO(2001)6).

[46] OECD, Acute oral toxicity – fixed dose procedure (chptr), Oecd Guidel. Test. Chem. (2001) 1–14, https://doi.org/10.1787/9789264070943-en.

[47] D.T. Hoagland, J. Liu, R.B. Lee, R.E. Lee, New agents for the treatment of drug-resistant Mycobacterium tuberculosis, Adv. Drug Deliv. Rev. 102 (2016) 55–72, https://doi.org/10.1016/j.addr.2016.04.026.

[48] D. Mahamed, M. Boulle, Y. Ganga, C. Mc Arthur, S. Skroch, L. Oom, O. Catinas, K. Pillay, M. Naicker, S. Rampersad, C. Mathonsi, J. Hunter, G. Sreejit, A.S. Pym, G. Lustig, A. Sigal, Intracellular growth of Mycobacterium tuberculosis after macrophage cell death leads to serial killing of host cells, Elife. 6 (2017) 1–25, https://doi.org/10.7554/eLife.22028.

[49] R. Fukuda, H. Nagasawa-Fujimori, Mechanism of the rifampicin induction of RNA polymerase beta and beta′ subunit synthesis in Escherichia coli, J. Biol. Chem. 258 (1983) 2720–2728. http://www.ncbi.nlm.nih.gov/entrez/query.fcgi?cmd=Retrieve&db=PubMed&dopt=Citation&list_uids=6296152.

[50] G. Griffiths, B. Nyström, S.B. Sable, G.K. Khuller, Nanobead-based interventions for the treatment and prevention of tuberculosis, Nat. Rev. Microbiol. 8 (2010) 827–834, https://doi.org/10.1038/nrmicro2437.

[51] R. Pandey, A. Zahoor, S. Sharma, G.K. Khuller, Nanoparticle encapsulated antitubercular drugs as a potential oral drug delivery system against murine tuberculosis, Tuberculosis. 83 (2003) 373–378, https://doi.org/10.1016/j.tube.2003.07.001.

[52] A. Delgado, E. Matijevie, Particle size distribution of inorganic colloidal dispersions: a comparison of different techniques, Part. Part. Syst. Charact. 8 (1991) 128–135.

[53] S. Honary, F. Zahir, Effect of zeta potential on the properties of nano-drug delivery systems - a review (part 2), Trop. J. Pharm. Res. 12 (2013) 265–273.

[54] S. Honary, F. Zahir, Effect of zeta potential on the properties of nano-drug delivery systems - a review (part 1), Trop. J. Pharm. Res. 12 (2013) 255–264.

[55] S. Hua, H. Ma, X. Li, H. Yang, A. Wang, pH-sensitive sodium alginate/poly(vinyl alcohol) hydrogel beads prepared by combined Ca^{2+} crosslinking and freeze-thawing cycles for controlled release of diclofenac sodium, Int. J. Biol. Macromol. 46 (2010) 517–523, https://doi.org/10.1016/j.ijbiomac.2010.03.004.

[56] C. Sartori, D.S. Finch, B. Ralph, K. Gilding, Determination of the cation content of alginate thin films by FTIR spectroscopy, Polymer (Guildf). 38 (1997) 43–51, https://doi.org/10.1016/S0032-3861(96)00458-2.
[57] K. Mladenovska, O. Cruaud, P. Richomme, E. Belamie, R.S. Raicki, M. Venier-julienne, E. Popovski, J.P. Benoit, K. Goracinova, 5-ASA Loaded Chitosan – Ca – Alginate Microparticles: Preparation and Physicochemical Characterization, 345, 2007 59–69, https://doi.org/10.1016/j.ijpharm.2007.05.059.
[58] P.W. Labuschagne, R. Adami, S. Liparoti, S. Naidoo, H. Swai, E. Reverchon, Preparation of rifampicin/poly(D,L-lactice) nanoparticles for sustained release by supercritical assisted atomization technique, J. Supercrit. Fluids 95 (2014) 106–117, https://doi.org/10.1016/j.supflu.2014.08.004.
[59] ISO (International Organization for Standardization), ISO 10993-5:2009: biological evaluation of medical devices—part 5: tests for in vitro cytotoxicity, Communication. (2009) https://doi.org/10.5594/J09750.
[60] U. Convention, The United States Pharmacopeia 30 the National Formulary, United States Pharmacopeial Convention, Rockville Md, 2007. http://www.worldcat.org/title/united-states-pharmacopeia-23-the-national-formulary-18-official-from-january-1-1995/oclc/465659387, Accessed date: 26 March 2018.
[61] J. Shetty Akhila, D. Shyamjith, M. Alwar, Acute toxicity studies and determination of median lethal dose, Curr. Sci. 93 (2007) 917–920, https://doi.org/10.2307/24099255.
[62] G. Zbinden, M. Flury-Roversi, Significance of the LDx50-test for the toxicological evaluation of chemical substances, Arch. Toxicol. 47 (1981) 77–99.